Proceedings of the 21st ICSMGE, Vienna, Austria, 14 – 19 June 2026. Pistrol, Adam & Schweiger (eds.)
Published by: ÖGG, Austrian Society for Geomechanics, Salzburg, Austria, ISBN 978-3-9503898-4-5
https://doi.org/10.53243/ICSMGE2026-1696

Impact of subsurface urban heat islands on the performance of pile foundations

Giulia Capati, Diana Salciarini
Department of Civil and Environmental Engineering, University of Perugia, Via G. Duranti 93, 06125 Perugia, Italy

Alessandro F. Rotta Loria
Subsurface Opportunities and Innovations Laboratory, SOIL, Department of Civil and Environmental Engineering, Northwestern University, 2145 Sheridan Road, Evanston, Illinois 60208, USA

ABSTRACT: Subsurface urban heat islands (SUHIs) represent a form of underground climate change caused by rising subsurface temperatures due to anthropogenic activity, increasingly affecting urban areas worldwide. This phenomenon has been observed and studied in several major cities, where it has been linked to environmental, public health, and transportation challenges. Recently, SUHIs have emerged as a subtle but significant threat to civil infrastructure, primarily due to thermally induced ground deformations. Despite the growing prevalence of this issue, a thorough investigation into its effects on the serviceability performance of geotechnical systems, such as deep foundations, remains largely unexplored. This study seeks to deepen the understanding of the impacts of SUHIs on the urban environment with a focus on the performance of pile foundations. To this aim, a building in the Chicago Loop district was selected as the case study. A detailed 3D computer model of the building foundation system and the surrounding ground was developed, informed by data gathered from laboratory tests on soil samples and a network of sensors distributed across various surface and subsurface environments within the district. This model served as the basis for simulations spanning a 100-year period, employing a time-dependent, 3D thermo-mechanical finite element modeling approach. The study evaluates the impact of rising subsurface temperatures on the mechanical performance of the building foundation system, focusing on key factors such as thermally induced stresses, deformations, and displacements. This study highlights that rising subsurface temperatures exert gradual yet continuous effects on the deformations and displacements of pile foundations, while causing minor variations in vertical stresses. Piles with significant temperature anomalies, located centrally within the foundation system, undergo greater deformations due to group effects. Heat released from the basement and street surface, accumulating underground, alters the modes and timing of concrete deformation. Over time, these persistent changes could potentially impact the building's performance.

KEYWORDS: Subsurface urban heat islands; Underground climate change; 3D Finite element modeling; Temperature effects; Pile foundations

1 INTRODUCTION

Climate change is increasingly highlighted as a growing concern not only for its atmospheric impacts but also for its effects below the surface (Ferguson & Woodbury, 2004; Epting & Huggenberger, 2013). One such manifestation is the progressive warming of the urban subsurface, commonly referred to as Subsurface Urban Heat Islands (SUHIs) phenomenon (Rotta Loria et al. 2022; Rotta Loria, 2023; Rotta Loria, 2024). Marked by elevated ground temperatures beneath densely built environments, this phenomenon originates from a combination of localized sources (such as underground structures, district heating systems, high-voltage power lines, and sewers) and more diffuse influences, including the surface urban heat island effect and global climate change (Menberg et al. 2013; Visser et al. 2020). Both types of drivers contribute to a gradual but persistent accumulation of heat in the ground. SUHIs have attracted growing scientific attention due to their implications for environmental sustainability (Benz et al. 2016; Bucci et al. 2017) public health, and the resilience of transportation infrastructure (Ampofo et al. 2004; Rotta Loria et al. 2022). At the same time, such phenomenon has attracted increasing interest in the energy sector, as it presents a valuable opportunity to recover and repurpose excess thermal energy stored in the urban subsurface for space heating in buildings and infrastructure systems (Bayer et al. 2019; Bidarmaghz et al. 2019).

Recently, subsurface urban heat islands have also been investigated within the field of civil engineering, based on the hypothesis that the warming of different soil types and construction materials may influence the mechanical behavior of civil structures and infrastructures in complex ways, potentially compromising the integrity and long-term performance of the built environment (Thota & Rotta Loria, 2025).

The present work aims to advance knowledge on how SUHIs affect urban systems, with particular attention to the behavior and performance of pile foundations. To this end, a representative building located in the Chicago Loop district was selected as a case study. A detailed three-dimensional (3D) numerical model of the foundation–soil system was developed, informed by temperature field data acquired through a network of sensors distributed throughout surface and subsurface environments in the area.

The model was used to perform long-term simulations over a 100-year period, employing a time-dependent, 3D thermo-mechanical finite element framework. The analysis investigates the effects of gradual subsurface temperature increases on the mechanical response of the foundation system, with particular emphasis on thermally induced stresses, strains, and displacements.

2 METHODOLOGY AND CASE ANALYSIS

2.1 *Temperature sensing network*

This work builds upon an extensive temperature monitoring campaign conducted in both surface and subsurface environments of Chicago's central Loop district, where the case study building is located. The building and monitoring network have been thoroughly described in previous studies (Rotta Loria et al. 2022; Rotta Loria, 2023). Beginning in 2019, a dense network of temperature sensors has been installed across the Chicago Loop district. This monitoring initiative was designed with three primary objectives: (1) collect high-resolution surface air temperature data for the downtown area, contributing to broader environmental monitoring efforts across Chicagoland and the state of Illinois; (2) investigate the correlations between surface air temperatures and those observed within subsurface built environments; and (3) directly

measure ground temperatures beneath the urban core of Chicago. The monitoring campaign spans a variety of urban settings. Surface measurements were taken in contrasting environments such as green parks and paved streets, while subsurface monitoring included a wide range of enclosed spaces, such as underground roadways, building basements across residential, commercial, and institutional facilities, as well as parking garages. One of the key outcomes of this effort was the identification of linear relationships between surface and subsurface air temperatures across the monitored built environments. These relationships provide a practical means to predict underground air temperatures based on known surface conditions, offering a useful basis for understanding and modeling the thermal behavior of subsurface urban spaces over time.

2.2 *Case study and numerical model*

The case study focuses on a recently renovated 39-storey Class A office building located in the highly regarded Central Loop/La Salle Street submarket of downtown Chicago. The structure is founded on a piled-slab system comprising 91 belled piles, directly derived from the traditional Chicago caisson method (Figure 1). This location provides an ideal context for investigating the impact of subsurface urban heat islands on geotechnical structures: recent studies have indeed reported subsurface temperature anomalies of up to 15 °C in the Chicago Loop area, compared to an undisturbed ground temperature of approximately 11 °C (Rotta Loria et al. 2022; Rotta Loria, 2023; Thota & Rotta Loria, 2025). These findings emphasize the significant influence of SUHIs, highlighting the relevance of this case study for investigating the effects of SUHI-induced temperature anomalies on the structural behavior of deep foundation systems.

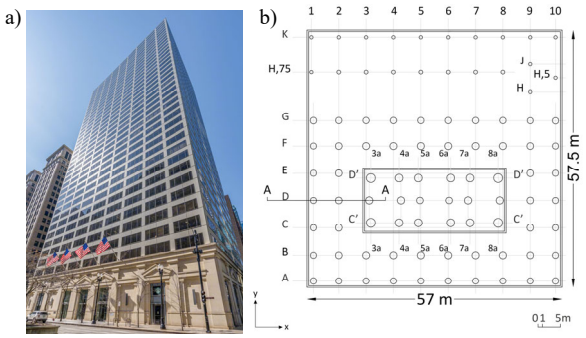

Figure 1. a) Chicago North La Salle office building; b) plan view of the foundations system.

Figure 2 illustrates the 3D computational model developed for the foundation system of the selected case study and informed by data collected from the network of temperature sensors described in Section 2.1. The model encompasses the underground level of the building, the foundation slab, and the supporting belled piles. The surrounding soil is modeled as a horizontally layered profile consisting of six distinct strata, whose thermo-physical and thermo-mechanical properties were derived from the literature (Rotta Loria, 2023) and are listed in Table 1 Table 2, along with all parameters adopted in the numerical simulations.

According to data provided by the Illinois State Geological Survey (2021), the stratigraphy comprises, from top to bottom: a surface sand layer (0–4 m), followed by soft clay (4–16 m), stiff clay (16–19 m), hard clay (19–27 m), a deposit of sand with boulders (27–34 m), and a dolomitic limestone bedrock beneath. The groundwater table is located at a depth of 4 meters.

This model served as the basis for long-term simulations over a 100-year period, using a time-dependent, 3D thermo-mechanical finite element approach. The simulations account for the interaction between heat transfer and the mechanical behavior of both the soil and the structural elements, allowing for the evaluation of long-term impacts of subsurface temperature anomalies on the stress–strain response of the foundation system. Simulations are run with COMSOL Multiphysics (v. 6.3).

Table 1. Thermo-physical properties of the ground underneath the Chicago Loop district.

Geological layer	Thermal conductivity, λ [W/(m°C)]	Heat capacity at constant pressure, c_p [J/(kg°C)]	Density, ρ [kg/m^3]
Sand	1	782	1918
Soft clay	1.22	1456	1846
Stiff clay	1.22	1456	2000
Hard clay	1.22	1456	2081
Sand and boulders	3	1035	2320
Dolomitic limestone	3	835	2639

Table 2. Thermo-mechanical properties of the ground underneath the Chicago Loop district.

Geological layer	Young's modulus, E [MPa]	Poisson's ratio, ν [-]	Linear thermal expansion coefficient, α [°C^{-1}]
Sand	31	0.2	$10 \cdot 10^{-5}$
Soft clay	10	0.2	$-9 \cdot 10^{-6}$
Stiff clay	31	0.2	$-9 \cdot 10^{-6}$
Hard clay	214	0.2	$9 \cdot 10^{-6}$
Sand and boulders	75	0.2	$10 \cdot 10^{-5}$
Dolomitic limestone	45586	0.1	$2.2 \cdot 10^{-6}$

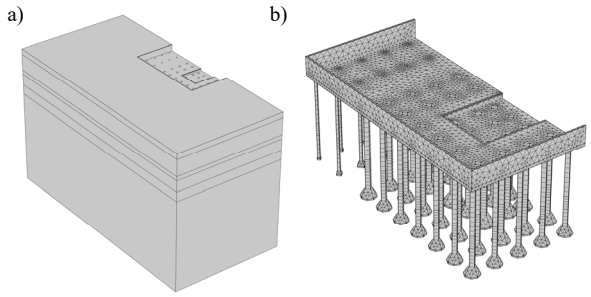

Figure 2. a) numerical model of the building foundation system and surrounding soil; b) finite element mesh of the foundation system.

Boundary conditions were calibrated using observed temperature trends to realistically reproduce the urban thermal environment (Rotta Loria et al. 2022) and will be discussed in the following Section. This modeling framework provides a robust platform for evaluating how sustained thermal

anomalies, such as those induced by SUHIs, can alter the performance, reliability, and design considerations of deep foundation systems in dense urban settings.

3 MATHEMATICAL FORMULATION

The mathematical formulation adopted in this study is well-suited for capturing complex thermo-mechanical phenomena involving heat transfer and deformation, such as those investigated in the present work.

The idealizations and assumptions underlying the numerical simulations are summarized as follows:

- Heat transfer in both the ground and the concrete forming the foundation system is assumed to occur solely through conduction. This assumption is appropriate in view of negligible groundwater flow and interconnected advection phenomena in the subsurface of the area.
- The ground is modeled as an isotropic and homogeneous medium exhibiting linear thermo-elastic behavior. Its displacements and deformations are described using a linear kinematic framework under quasi-static conditions. For normally consolidated clays, thermal collapse is taken into account in an approximate manner by considering a negative thermal expansion coefficient, as fine-grained soils tend to undergo volumetric contraction when heated under three-dimensional conditions (Laloui, 2001). The porous medium is assumed to have pores filled with a fluid (e.g., water or air), and its overall thermophysical properties arise from the combined characteristics of both the solid and fluid phases.
- The concrete is idealized as an isotropic and homogeneous material exhibiting time-dependent viscoelastic behavior, which is governed by the Generalized Kelvin–Voigt model.
- The governing equations for heat transfer and mechanical deformation (namely, the continuity equation and the energy conservation equation) are numerically coupled within a time-dependent simulation framework.

3.1 *Heat transfer*

The energy conservation equation allowing modeling the purely conductive heat transfer within the foundation system and the surrounding ground reads:

$$\lambda \nabla^2 T = \rho c_p \frac{\partial T}{\partial t} \tag{1}$$

where λ denotes the thermal conductivity of the material (determined, for the soil layers, via the material porosity, n, through the thermal conductivity of water λ_w or air λ_a, and the thermal conductivity of the solid particles λ_s), ∇^2 is the Laplacian operator, ρ is the density of the material (for the soil layers, similarly estimated through the density of water ρ_w or air ρ_a, and the density of the solid particles ρ_s) and c_p represents the specific heat of the material (for the soil layers, calculated through the specific heat of water $c_{p,w}$ or air $c_{p,a}$ and the specific heat of the solid particles $c_{p,s}$).

3.2 *Deformation phenomena*

The momentum conservation equation, expressed in the form of a simplified static equilibrium equation is given by:

$$\nabla \cdot \sigma_{ij} = 0 \tag{2}$$

where σ_{ij} represents the total stress tensor, which can be expressed as follows:

$$\sigma_{ij} = D_{ijkl} \left[\varepsilon_{kl} + \beta_{kl} \left(T - T_0\right)\right] \tag{3}$$

where D_{ijkl} is the elastic stiffness tensor, which includes the material parameters (such as Young's modulus, E, and Poisson's ratio, ν) , ε_{kl} denotes the total strain tensor, the vector β_{kl} contains the linear thermal expansion coefficient of the material, α, and $T - T_0 = \Delta T$ represents the applied temperature variation. In the formulation of Eq. (2), body forces are neglected, as the analyses are intended to capture the incremental thermo-mechanical response (i.e., variations in stress and displacement induced by temperature changes) assuming an initial state already in equilibrium under self-weight.

The viscoelastic creep behavior of concrete, i.e., its tendency to undergo continued deformation under sustained load, is incorporated into the model to enhance the realism of the simulation, given both the extended time span of the study (100 years) and the sensitivity of this phenomenon to thermal variations.

The Kelvin chain approach is the preferred theoretical viscoelastic model to describe the creep of concrete, where there is an increase in strain under constant stress (Pomarico et al. 2016). Specifically, the Generalized Kelvin Voigt (GKV) model includes a series configuration of n Kelvin-Voigt branches, where each branch comprises a spring (characterized by modulus G_i) and a damper (with viscosity coefficient η_i).

Through the utilization of a GKV model, the specific creep function, at a given loading instant t_0, can be described by the following function:

$$J(t - t_0) = \frac{1}{G_0} + \sum_{i=1}^{n} \frac{1}{G_i}\left[1 - e^{\frac{t - t_0}{\tau_i}}\right] \tag{4}$$

$$\tau_i = \frac{\eta_i}{G_i} \tag{5}$$

The parameter τ_i is the retardation time per branch, i.e. an estimate of the time required for the creep process to approach completion, with reference to the *i-th* branch.

In such a model, the stress at each unit is the same external stress, whereas the total strain is the sum of the elastic strain of the first spring ε_{el} plus the strains of the branches:

$$\varepsilon = \varepsilon_{el} + \sum_{i=1}^{n} \varepsilon_i \tag{6}$$

Table 3. Viscoelastic parameters used in the viscoelastic branches for the concrete.

Viscoelastic branch	Elastic modulus, E [MPa]	Shear modulus, G [MPa]	Relaxation time, τ [s]
1	76164	25388	5e2
2	108805	36268	5e3
3	87044	29015	5e4
4	54403	18134	5e5
5	32642	10881	5e6
6	43522	14507	5e7
7	65283	21761	5e8
8	65283	21761	5e9

It can be demonstrated that each Kelvin-Voigt branch obeys a differential equation relating the stress to the strain and its derivative (Marques & Creus, 2012). In the multiaxial stress case, the differential equation has the following expression:

$$\tau_i \dot{\varepsilon}_i + \varepsilon_i = \frac{1}{2G_i}\sigma_{dev} \tag{7}$$

where σ_{dev} is the deviatoric stress tensor.

Since no experimental data on the viscoelastic behavior of the concrete used in the case-study foundation were available, the parameters proposed by Pomarico et al. (2016) were adopted, assuming a generic concrete with comparable properties. This assumption is further supported by the similar compressive strength of the two materials.

The viscoelastic parameters adopted for the eight viscoelastic branches of the GKV model used to represent concrete behavior are reported in Table 3.

3.3 *Initial and boundary conditions*

The numerical model is illustrated in Figure 2. The model utilizes a tetrahedral mesh composed of 121177 domain elements and 7300 edge elements. The initial and boundary conditions required for solving the problem are detailed below and illustrated in Figure 3.

The thermal initial conditions assume a uniform ground temperature of $T_{0,g}$ = 11.2 °C, based on data collected from the deployed sensing network described in Section 2.1. The mechanical initial conditions consist of zero initial displacements and no externally applied forces.

Thermal boundary conditions are defined as follows:

- A time-dependent temperature is applied to the top surface of the model, representing the thermal environmental conditions at the street level. This input follows the surface temperature profile proposed by Rotta Loria et al. (2022), who derived it using the model by Baggs (1983) and historical and projected surface air temperature data from 1951 to 2051 provided by the National Oceanic and Atmospheric Administration (US Department of Commerce, NOAA, 2022).
- A time-varying temperature is also imposed on the walls of the basement of the building, based on empirical relationships between surface and subsurface air temperatures obtained through the sensing network, representing the thermal conditions in such underground environment (Rotta Loria et al. 2022).
- A constant temperature of $T_{0,g}$ = 11.2 °C is enforced on the bottom and lateral boundaries of the model domain, representing the far field conditions.

Mechanical boundary conditions consist of the following:

- The bottom surface is subjected to a fixed constraint, representing the unyielding nature of the underlying limestone layer ($u = 0$).
- For the side surfaces of the geological model, a roller constraint is employed ($u \cdot n = 0$), permitting lateral movement of the entire volume while inhibiting movement perpendicular to the surfaces.

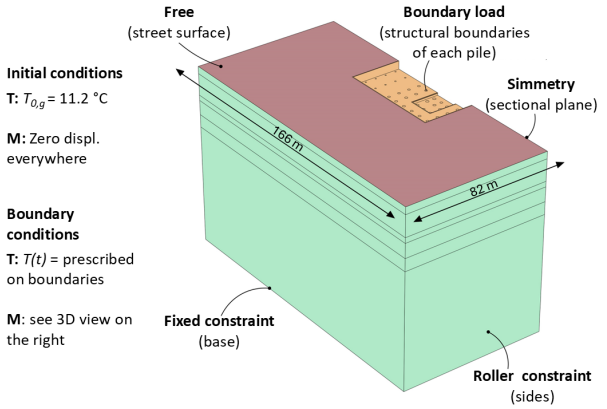

Figure 3. Schematic of initial and boundary conditions assumed in the modeled problem.

- The building load was distributed among the caissons based on estimates from the serviceability limit state load calculation. For each pile, a force proportional to the diameter of its enlarged base was assigned.
- No explicit interface elements were introduced between the piles and the surrounding soil. The two domains are directly connected, assuming full continuity of displacements and stresses at the pile–soil contact.

4 RESULTS AND DISCUSSION

The thermal and mechanical behavior of the foundation system in the present case study has been analyzed in terms of temperature, vertical displacements, and vertical stresses, focusing on three selected piles chosen for their representative positions within the foundation layout: one located at a corner, one along the edge of the system and one in a central position. These are indicated in yellow, orange, and red, respectively, in the foundation plan diagrams shown in each of the following figures.

4.1 *Temperature*

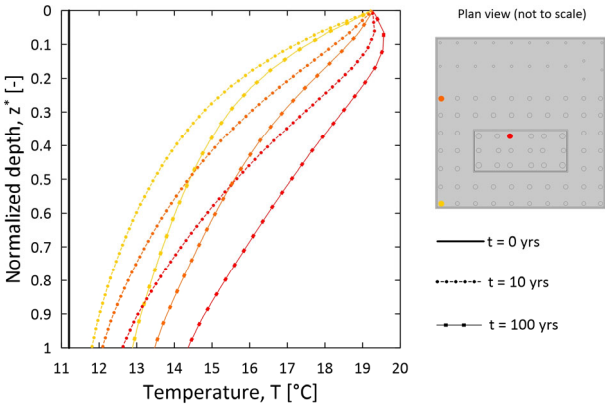

Figure 4. Temperature profiles along the axes of the three foundations considered for the analysis after simulation times of t = 0, 10 and 100 years.

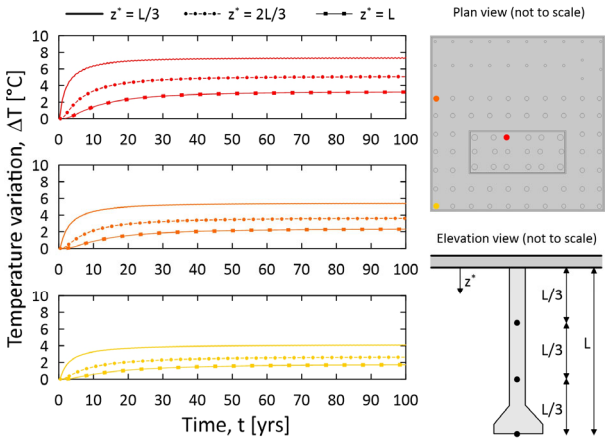

Figure 5. Temperature variation trends over time for three points at depths $z^* = L/3$, $2L/3$ and L of the three foundations considered.

Figure 4 illustrates the temperature trend along the axes of the three selected foundations mentioned in the previous paragraph, after simulation times of t = 0, 10 and 100 years. Here and in the following graphs, the depth of the foundations has been normalized with respect to the corresponding length of the three piles.

As can be noted, for each pile, the highest temperature is found near the pile head due to its proximity to the basement, where the specified temperature boundary was applied. The central pile shows the highest temperature rise, especially in its upper part, likely due to its greater exposure to basement heat. The magnitude of temperature increase appears to decrease as pile's position becomes more peripheral within the foundation layout.

Figure 5 confirms that temperature increases are more pronounced in piles with greater exposure to basement heat. For all piles, temperatures rise rapidly during the first 10 years before stabilizing. Both the temperature rise and its rate clearly decrease with depth, reflecting the underlying heat diffusion dynamics in the subsurface.

4.2 *Vertical displacements*

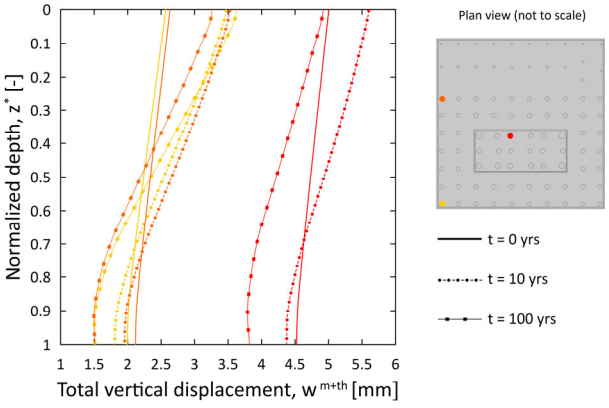

Figure 6. Vertical displacements trends along the axes of the three foundations considered for the analysis after simulation times of t = 0, 10 and 100 years.

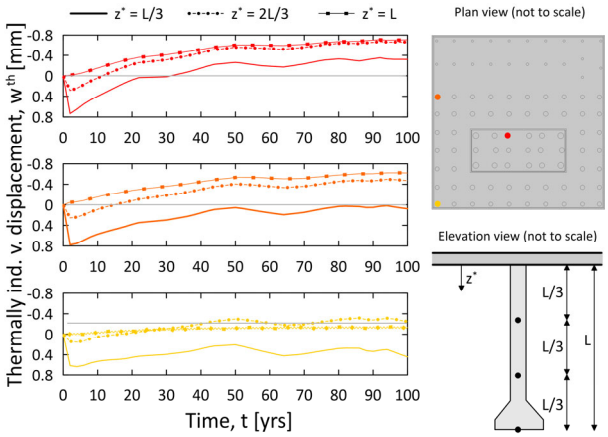

Figure 7. Vertical displacement variation trends over time for three points at depths $z^* = L/3$, $2L/3$ and L of the three foundations considered.

Figure 6 shows vertical displacement profiles along the axes of the three foundations analyzed after simulation times of t = 0, 10 and 100 years. Positive values indicate downward displacements, while negative values indicate upward displacements. The central foundation shows the greatest initial settlement due to the applied mechanical load. After 10 years, all three foundations exhibit vertical settlement along the upper two-thirds of their depth, followed by uplift in the lower third. After 100 years, the uplift becomes more pronounced, eventually resulting in an overall upward displacement of the entire foundation. As shown in Figure 7, this behavior evolves over time and varies with depth. The initial contraction, especially near the top, may be linked to concrete creep under sustained load. In the long term, however, thermal expansion of the deeper hard clay layer appears to drive the progressive uplift. Although displacements remain small (up to 0.8 mm), they are continuous and likely influenced by the mechanical and thermal properties of the surrounding soils.

4.3 *Vertical stresses*

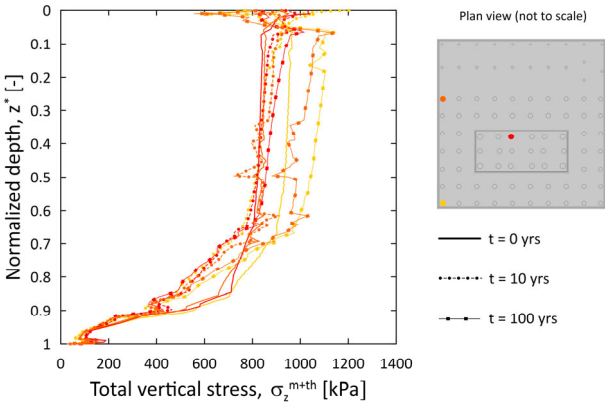

Figure 8. Vertical stress trends along the axes of the three foundations considered after simulation times of t = 0, 10 and 100 years.

Figure 8 shows vertical stress trends along the axes of the three foundations analyzed, after simulation times of t = 0, 10 and 100 years, while Figure 9 illustrates the evolution of thermally induced stress trends over time at three different depths of each pile. For all piles, an inverse behavior is observed between the upper portion (approximately up to 0.7L) and the deeper section. After 100 years, compressive stresses increase in the upper parts of all piles, especially for the side and corner ones.

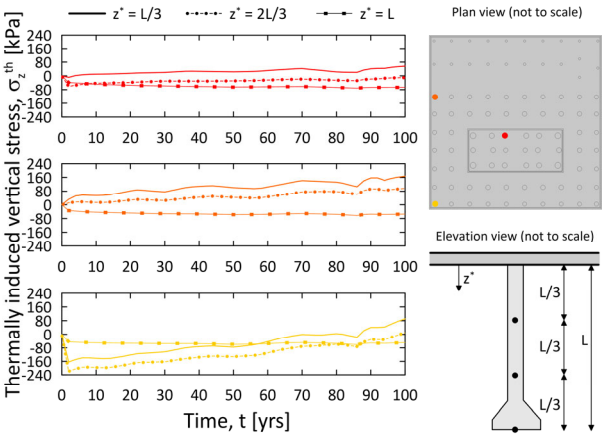

Figure 9. Thermally induced vertical stress trends over time for three points at depths $z^* = L/3$, $2L/3$ and L of the three foundations considered.

The corner pile initially shows tensile stresses (after 10 years), which progressively shift to compression over time. This stress inversion is likely driven by the response of the three soil layers: the upper two-thirds, composed of soft and stiff clays, tend to contract with heating, while the deeper hard clay expands, generating tensile stresses. Between 0 and 100 years, compressive stresses increase by ~200 kPa for the corner and side piles, and by ~100 kPa for the central pile. Figure 9 supports the findings from Figure 8, confirming the tendency of the upper pile sections to develop increasing thermally induced compressive stresses. Notably, only the corner pile exhibits tensile stresses during the early stages of the analysis.

5 FINAL REMARKS

This study contributes to the growing research on Subsurface Urban Heat Islands (SUHIs), an increasingly relevant issue in densely built environments, by investigating its potential impact on pile foundation systems. It focuses on a case-study building in the Chicago Loop district, where elevated subsurface temperatures have been associated with ground deformations. The analysis examines how heat emissions from the basement affect the mechanical behavior of the supporting foundations, specifically in terms of temperature distribution, vertical displacements, and stress variations, with the aim of improving the understanding of SUHIs-related risks to urban infrastructure.

Based on the obtained results, it is possible to summarize the following key aspects:

- The heat distribution emitted from the basement does not affect all parts of the foundation uniformly. The central pile exhibits the highest temperatures, while the thermal influence diminishes for the side and corner piles.
- Thermally induced vertical displacements reflect the observed temperature patterns. The central pile experiences the largest displacements, influenced both by higher temperatures and greater mechanical loading. In contrast, the corner pile shows smaller displacements, where the effect of the surrounding soil behavior becomes more dominant.
- Vertical stress variations are substantially influenced not only by temperature but also by the thermo-mechanical behavior of the surrounding soil layers. In the upper sections of the piles, embedded in normally consolidated clay that contracts when heated, compressive stresses increase. In the deeper sections, where the piles are in contact with hard clay, this trend is mitigated, and tensile stresses may develop.

This study highlights the complexity of the long-term mechanical behavior of deep foundations in the context of SUHIs. Thermally induced effects are slow but continuous, and their magnitude strongly depends on both the intensity of the thermal source and the specific properties of the surrounding soils. These characteristics make long-term consequences difficult to predict without detailed analysis and emphasize the importance of investigating the phenomenon, as its persistent and complex nature can significantly affect the performance of urban infrastructure over time.

6 REFERENCES

Ferguson, G. & Woodbury, A. D. 2004. Subsurface heat flow in an urban environment. *J. Geophys. Res. Solid Earth* 109, B02402.

Epting, J. & Huggenberger, P. 2013. Unraveling the heat island effect observed in urban groundwater bodies–Definition of a potential natural state. *J. Hydrol.* 501, 193–204.

Rotta Loria, A. F., Thota, A., Thomas, A. M., Friedle, N., Lautenberg, J. M., and Song, E. C. 2022. Subsurface heat island across the Chicago Loop district: Analysis of localized drivers. *Urban Climate* 44, 101211.

Rotta Loria, A. F. 2023. The silent impact of underground climate change on civil infrastructure. *Communications Engineering* 44.

Rotta Loria AF. Open questions about the effects of ground warming on infrastructure. 2024. *Nature Cities* 1, 12, 804-807.

Menberg K, Bayer P, Zosseder K, Rumohr S, Blum P. 2013. Subsurface urban heat islands in German cities. *Sci Total Environ.* 442, 123–133.

Visser PW, Kooi H, Bense V, Boerma E. 2020. Impacts of progressive urban expansion on subsurface temperatures in the city of Amsterdam. (The Netherlands). *Hydrogeol J.* 28, 5, 1755–1772.

Benz, S. A., Bayer, P., Goettsche, F. M., Olesen, F. S. & Blum, P. 2016. Linking surface urban heat islands with groundwater temperatures. *Environ. Sci. Technol.* 50, 70–78.

Bucci, A., Barbero, D., Lasagna, M., Forno, M. G. & De Luca, D. A. 2017. Shallow groundwater temperature in the Turin area (NW Italy): vertical distribution and anthropogenic effects. *Environ. Earth Sci.* 76, 221.

Ampofo F, Maidment G, Missenden J. 2004. Underground railway environment in the UK: part 3: methods of delivering cooling. *Appl Therm Eng.* 24, 5, 647–659.

Bayer, P., Attard, G., Blum, P., & Menberg, K. 2019. The geothermal potential of cities. *Renewable and Sustainable Energy Reviews* 106, 17-30.

Bidarmaghz, A., Choudhary, R., Soga, K., Kessler, H., Terrington, R. L., & Thorpe, S. 2019. Influence of geology and hydrogeology on heat rejection from residential basements in urban areas. *Tunnelling and Underground Space Technology* 92, 103068.

Thota, A. N., & Rotta Loria, A. F. 2025. Quantifying Creeping Deformations due to Subsurface Urban Heat Islands in Chicago. In Geotechnical Frontiers 2025, 30-38.

Illinois State Geological Survey, 2021. Illinois Water and Related Wells. [Online] Available at: https://prairieresearch.maps.arcgis.com/apps/webappviewer/index.html?id=e06b64ae0c814ef3a4e43a191cb57f87 [Accessed 2021].

Laloui, L. 2001. Thermo-mechanical behaviour of soils. *Rev Fr Génie Civ.* 5, 6, 809–843.

Marques, S. P., and Creus, G. J. 2012. *Computational Viscoelasticity*. Springer Science & Business Media.

Pomarico, A. A., Roselli, G., & Caltabiano, D. 2016. Modelling of viscoelastic phenomena in concrete structures. *Proc. of the 2016 COMSOL conference*, Munich.

Baggs, S. A. 1983. Remote prediction of ground temperature in Australian soils and mapping its distribution. *Sol. Energy* 30, 351–366.

US Department of Commerce. National Oceanic and Atmospheric Administration (NOAA), 2022. National Weather Service – Climate data for Chicago. [Online] Available at: https://www.weather.gov/wrh/Climate?wfo=lot [Accessed 2022].